Research Article | Vol. 25, No. 23 | 13 Nov 2017 | OPTICS EXPRESS 28451
Optics EXPRESS

Broadband guided-mode resonant reflectors with quasi-equilateral triangle grating profiles

SHANWEN ZHANG,[1,*] YEONG HWAN KO,[2] AND ROBERT MAGNUSSON[2]

[1]*National Engineering Research Center for Diffraction Gratings Manufacturing and Application, Changchun Institute of Optics and Fine Mechanics and Physics, Chinese Academy of Sciences, Changchun, Jilin, 130033, China*
[2]*Department of Electrical Engineering, University of Texas at Arlington, Box 19016, Arlington, Texas 76019, USA*
[*]*zhshwen007@163.com*

Abstract: We present the design of broadband guided-mode resonant reflectors consisting of a grating layer with quasi-equilateral grating profiles and a homogeneous layer made of silicon on glass. Using the coordinate-transformation-based differential method of Chandezon (the C method) to determine the optimized base angles of the grating and thickness of the homogeneous layer, we arrive at example reflector designs for TM polarization. We quantify the effects of deviation of the parameters, simulate the inner magnetic field distribution at resonance wavelengths, and compute the tolerance in the incident angle of the optimized broadband reflector. For broadband structures with different thicknesses of the homogeneous layer, the base angles of the triangles are all close to 60°. The optimized reflector has reflectance of $R_0 > 99\%$ across a 567 nm bandwidth in the 1432-1999 nm wavelength range with fractional bandwidth of $\Delta\lambda/\lambda_{center} \approx 33.3\%$. Base angles play a critical role in determining the reflection bandwidth and the quasi-equilateral triangle profile is found to be the optimal configuration. This model can be used to design broadband guided-mode resonant reflectors operating in different spectral bands and guide the fabrication of these devices with diamond-tip based grating ruling engines.

OCIS codes: (050.1950) Diffraction gratings; (130.2790) Guided waves; (050.6624) Subwavelength structures.

References and links

1. L. Mashev and E. Popov, "Zero order anomaly of dielectric coated gratings," Opt. Commun. **55**, 377–380 (1985).
2. G. A. Golubenko, A. S. Svakhin, V. A. Sychugov, and A. V. Tishchenko, "Total reflection of light from a corrugated surface of a dielectric waveguide," Sov. J. Quantum Electron. **15**, 886–887 (1985).
3. R. Magnusson and S. S. Wang, "New principle for optical filters," Appl. Phys. Lett. **61**, 1022–1024 (1992).
4. S. S. Wang and R. Magnusson, "Theory and applications of guided-mode resonance filters," Appl. Opt. **32**(14), 2606–2613 (1993).
5. Y. Ding and R. Magnusson, "Resonant leaky-mode spectral-band engineering and device applications," Opt. Express **12**(23), 5661–5674 (2004).
6. D. Gerace and L. C. Andreani, "Gap maps and intrinsic diffraction losses in one-dimensional photonic crystal slabs," Phys. Rev. E Stat. Nonlin. Soft Matter Phys. **69**(5 Pt 2), 056603 (2004).
7. S. Boonruang, A. Greenwell, and M. G. Moharam, "Multiline two-dimensional guided-mode resonant filters," Appl. Opt. **45**(22), 5740–5747 (2006).
8. Y. Kanamori, T. Kitani, and K. Hane, "Guided-mode resonant grating filter fabricated on silicon-on-insulator substrate," Jpn. J. Appl. Phys. **45**, 1883–1885 (2006).
9. C.-L. Hsu, Y.-C. Liu, C.-M. Wang, M.-L. Wu, Y.-L. Tsai, Y.-H. Chou, C.-C. Lee, and J.-Y. Chang, "Bulk-micromachined optical filter based on guided-mode resonance in silicon-nitride membrane," J. Lightwave Technol. **24**, 1922–1928 (2006).
10. R. Magnusson and M. Shokooh-Saremi, "Physical basis for wideband resonant reflectors," Opt. Express **16**(5), 3456–3462 (2008).
11. M. C. Y. Huang, Y. Zhou, and C. J. Chang-Hasnain, "A surface-emitting laser incorporating a high index-contrast subwavelength grating," Nat. Photonics **1**, 119–122 (2007).
12. P. Cheben, S. Janz, D.-X. Xu, B. Lamontagne, A. Delâge, and S. Tanev, "A broad-band waveguide grating coupler with a subwavelength grating mirror," IEEE Photonics Technol. Lett. **18**, 13–15 (2006).

#302741 https://doi.org/10.1364/OE.25.028451
Journal © 2017 Received 19 Jul 2017; revised 25 Sep 2017; accepted 28 Sep 2017; published 2 Nov 2017

Optics EXPRESS

13. C. J. Chang-Hasnain, Y. Zhou, M. C. Y. Huang, and C. Chase, "High-contrast grating VCSELs," IEEE J. Sel. Top. Quantum Electron. **15**, 869 (2009).
14. C. C. Wang and S. D. Lin, "Resonant cavity-enhanced quantum-dot infrared photodetectors with sub-wavelength grating mirror," J. Appl. Phys. **113**, 213108 (2013).
15. T. Khaleque, M. J. Uddin, and R. Magnusson, "Design and fabrication of broadband guided-mode resonant reflectors in TE polarization," Opt. Express **22**(10), 12349–12358 (2014).
16. C. F. R. Mateus, M. C. Y. Huang, Y. Deng, A. R. Neureuther, and C. J. Chang-Hasnain, "Ultrabroadband mirror using low-index cladded subwavelength grating," IEEE Photonics Technol. Lett. **16**, 518–520 (2004).
17. Y. Ding and R. Magnusson, "Resonant leaky-mode spectral-band engineering and device applications," Opt. Express **12**(23), 5661–5674 (2004).
18. M. Shokooh-Saremi and R. Magnusson, "Wideband leaky-mode resonance reflectors: Influence of grating profile and sublayers," Opt. Express **16**(22), 18249–18263 (2008).
19. R. Magnusson and M. Shokooh-Saremi, "Physical basis for wideband resonant reflectors," Opt. Express **16**(5), 3456–3462 (2008).
20. H. Wu, J. Hou, W. Mo, D. Gao, and Z. Zhou, "A multilayer-based high-performance multisubpart profile grating reflector," IEEE Photonics Technol. Lett. **22**, 203–205 (2010).
21. C. J. Chang-Hasnain and W. Yang, "High-contrast gratings for integrated optoelectronics," Adv. Opt. Photonics **4**, 379–440 (2012).
22. H. Wu, L. Huang, Y. Xiao, C. Zhang, S. Li, N. Luo, X. He, and Y. Gao, "A wideband reflector realized by a subwavelength multi-subpart profile grating structure," J. Opt. **15**, 035703 (2013).
23. R. Magnusson, "Wideband reflectors with zero-contrast gratings," Opt. Lett. **39**(15), 4337–4340 (2014).
24. W. Yu, M. Ye, and Y. S. Yi, "Impacts of tapered sidewall profile on subwavelength grating wideband reflectors," J. Nanophotonics **9**, 093058 (2015).
25. X. Y. Wenxi and Y. Yi, "Impacts of tapered sidewall profiles with high aspect ratio on subwavelength grating structure," IEEE Photonics Technol. Lett. **27**, 1437–1440 (2015).
26. X. Li, H. Yu, X. Qi, S. Feng, J. Cui, S. Zhang, Jirigalantu, and Y. Tang, "300 mm ruling engine producing gratings and echelles under interferometric control in China," Appl. Opt. **54**, 1819–1826 (2015).
27. C. Yang, X. Li, H. Yu, H. Yu, J. Zhu, S. Zhang, and J. Gao, "Practical method study on correcting yaw error of 500 mm grating blank carriage in real time," Appl. Opt. **54**, 4084–4088 (2015).
28. Jirigalantu, X. Li, S. Zhang, X. Mi, J. Gao, Bayanheshig, X. Qi, and Y. Tang, "Ruling of echelles and gratings with a diamond tool by the torque equilibrium method," Appl. Opt. **55**, 8082–8088 (2016).
29. S. Zhang, X. Mi, Q. Zhang, Jirigalantu, S. Feng, H. Yu, and X. Qi, "Groove shape characteristics of echelle gratings with high diffraction efficiency," Opt. Commun. **387**, 401–404 (2017).
30. J. Chandezon, D. Maystre, and G. Raoult, "A new theoretical method for diffraction gratings and its numerical application," J. Opt. **11**, 235–241 (1980).
31. J. Chandezon, M. T. Dupuis, G. Cornet, and D. Maystre, "Multicoated grating: a differential formalism applicable in the entire optical region," J. Opt. Soc. Am. **72**, 839–846 (1982).
32. L. Li, J. Chandezon, G. Granet, and J. P. Plumey, "Rigorous and efficient grating-analysis method made easy for optical engineers," Appl. Opt. **38**(2), 304–313 (1999).

1. Introduction

Broadband reflectors based on guided-mode resonance (GMR) effects [1–10], having reflectance higher than 99% over a wide spectral range of $\Delta\lambda/\lambda_{center}$ exceeding 30%, are of interest for applications in lasers, couplers, and resonant cavity-enhanced photodetectors [11–14]. Possessing reflectance higher than metal mirrors and with structure being simpler than multilayer dielectric-stack mirrors motivates their development [15]. Numerous other applications have been realized with this basic resonance effect including biosensors, tunable filters, absorption enhanced solar cells, and nanoelectromechanical displays. Most of the previous works focus on structures with rectangular profiles due to their favorable spectral characteristics and straightforward fabrication using masks with dry etching [16–23]. Recently, broadband GMR structures and subwavelength gratings with trapezoidal profiles were designed and studied showing that tapered sidewall profiles will reduce the bandwidth and the overall reflectance [24-25]. Moderate tapers sometimes form during etching of resonant reflectors with planned rectangular profiles.

In this paper, we focus on the properties of broadband GMR reflectors with isosceles triangle grating profiles. The motivation for this work is planned fabrication with mechanical inscribing methods thus avoiding masking/etching steps. Quantification of the properties of such structures, not presently existing in the literature to our knowledge, is needed. Hence, we discuss the effects of the refractive index of the grating layer, base angles of the grating, and thickness of the homogeneous layer on the spectral reflectance. We find that the optimized

Optics EXPRESS

base angles of the grating triangles are close 60°, i.e. the structures with quasi-equilateral triangle grating profiles are the best ones. These results will be used to guide fabrication of broadband GMR reflectors with triangle grating profiles by grating ruling engines with diamond tools [26–29]. We note that broadband reflectors are readily designed to operate in various spectral bands by scaling the device design with the incident wavelength by changing the grating period. Thus, these results apply broadly in long-wave bands where mechanical ruling methods are well developed.

2. Device structures

Figures 1(a) and 1(b) show two types of GMR structures with the symmetric triangle (or isosceles) grating profiles treated here. They are air-grating-glass elements, so we fix the refractive index of the cover and substrate as n_c = 1 and n_s = 1.48 separately. Figure 1(a) illustrates a zero-contrast grating (ZCG) with a transition layer made of the same material as the grating layer between the grating layer and the substrate [23]. Figure 1(b) defines a high-contrast grating (HCG) with a discontinuous refractive index between the grating layer and the substrate [21]. In the figure, the left base angle of the grating α is equal to the right angle β corresponding to the thickness of the grating d_g, the homogenous-layer thickness is d_h, and the period is Λ. Therefore, α, d_h, n and Λ are the design parameters which should be optimized to achieve high reflectance across wide flat bands. As the period Λ determines primarily whether the spectral band locates at short or long wavelengths and our focus is on the optical communication band, it is fixed at 850 nm.

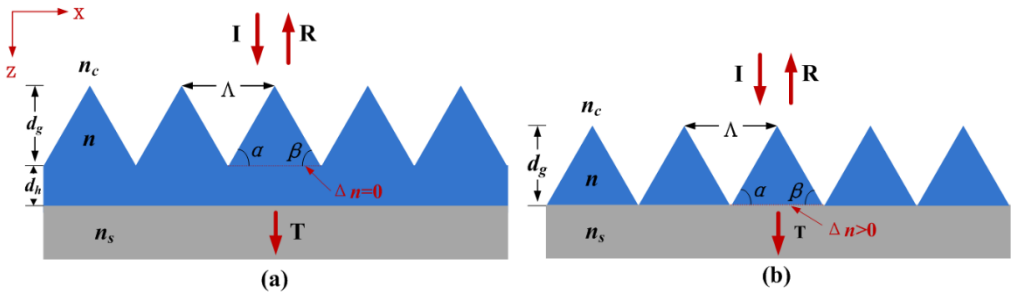

Fig. 1. Schematic model of broadband GMR reflectors with symmetric triangular grating profiles. (a) Zero-contrast grating structure with Δn = 0. (b) High-contrast grating structure with $\Delta n > 0$. The structures are made of a high index layer with n on a glass substrate with n_s = 1.48 and the cover index is n_c = 1 for incidence in air. I represents the incident plane wave, R denotes reflectance, and T labels the transmittance.

3. Numerical methods and assumptions

The software used in designing and optimizing these structures is DELTA which is based on the coordinate-transformation-based differential method of Chandezon [30-31]. DELTA [32] is a computer program for modeling multilayer-coated, surface-relief diffraction gratings of arbitrary permittivity in conical mountings. DELTA is well suited to treat gratings with smooth profiles, triangular profiles, and coated profiles. The incident light is assumed to be a monochromatic plane wave of infinite extent. All media in the layers are assumed to be isotropic, nonmagnetic, and homogenous. The polarization of the incident plane wave that we treat in this paper is TM, namely, the direction of the electric-field vector is parallel to the x-axis.

Optics EXPRESS

4. Design and results

4.1 Effects of key design parameters

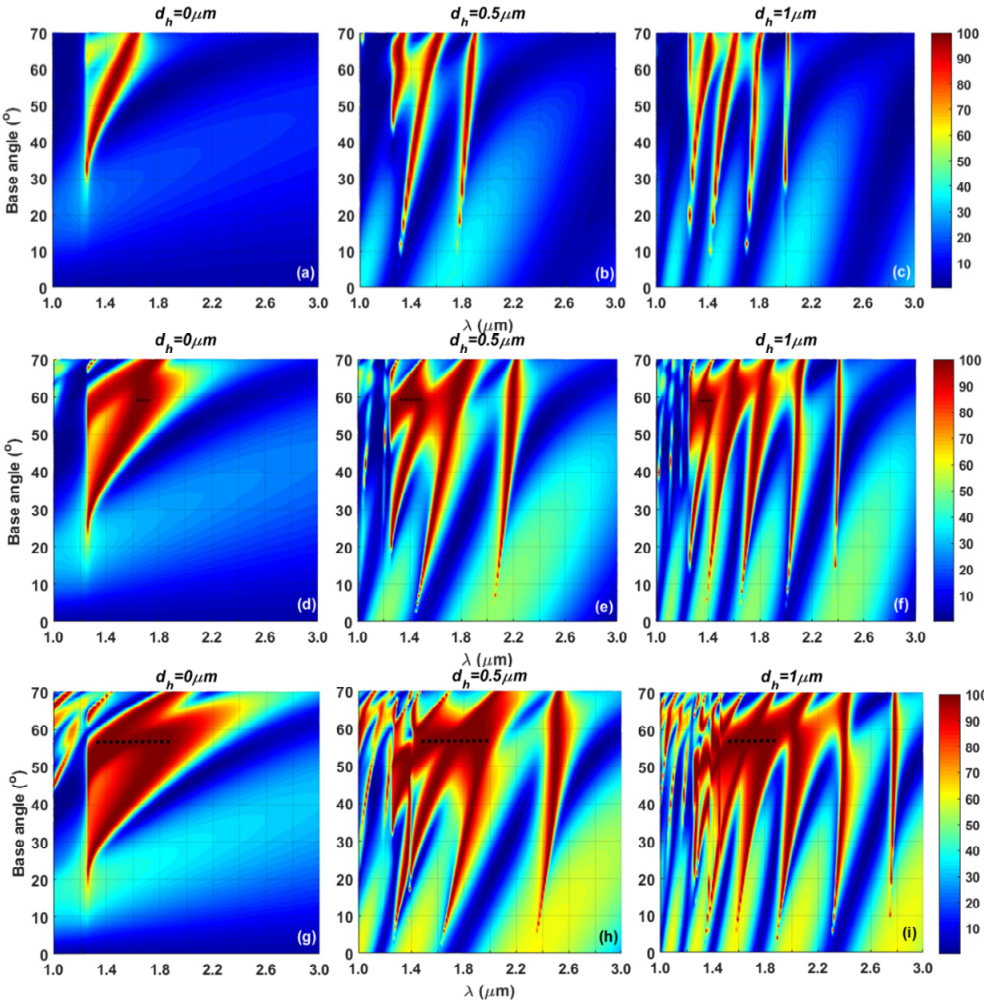

Fig. 2. Reflectance map R_0 (λ, α) drawn versus wavelength and base angle of the structure with triangle groove profiles for Λ = 850 nm, n_c = 1, and n_s = 1.48. (a)-(c) with n = 2.5, (d)-(f) with n = 3 and (g)-(i) with n = 3.48 for three homogenous-layer thicknesses d_h = 0 μm, 0.5 μm, and 1 μm separately.

The width of the high reflectance broadband, rooted in the distribution of resonant modes, is mainly affected by the grating layer and the homogenous layer including the geometrical parameters and refractive indices of the structures. We compute the reflectance map drawn versus wavelength and base angle of the grating with different homogenous-layer thickness of GMR gratings for three refractive indices n corresponding to three refractive index differences $\Delta n = n\text{-}n_s$ from the low to the high in Figs. 2(a)-2(i). We note that the grating thickness is related to the base angle. Figures 2(a)-2(c) are for a refractive index of n = 2.5 with low Δn, Figs. 2(d)-2(f) are for a refractive index n = 3 with medium Δn, and Figs. 2(h)-2(i) are for n = 3.48 with high Δn while the homogenous-layer thicknesses are 0 μm, 0.5 μm and 1 μm respectively. The middle parts of the red areas with high reflectance in each map represent the distribution of the resonant fundamental mode at long wavelengths and higher-order modes at shorter wavelengths. Figure 2(a) without a homogenous-layer due to d_h = 0,

Optics EXPRESS

i.e. HCG structure, shows that only the fundamental waveguide mode exists. Figures 2(b) and 2(c) with homogenous layers with d_h = 0.5 μm and 1 μm, i.e. ZCG structures, show that the fundamental mode shifts to a longer wavelength and higher order modes arise with increasing thickness of the homogenous layer. Refractive index of 3.48 corresponds to silicon and parts of the spectra cover the telecommunications region around the 1550 nm wavelength.

For the middle-valued refractive index difference Δn, Figs. 2(d)-2(f) show that the red areas with high reflectance are broader than for the low Δn case. Further increasing the refractive index difference Δn, Figs. 2(g)-2(i) show the broadest bands as expected. The broadband with high reflectance in black dashed lines in Figs. 2(d)-2(f) all correspond to the base angles of ~59° though the bandwidths differ. The fundamental mode will shift to longer wavelengths with additional higher-order modes arising on increasing the homogenous-layer thickness. Similarly, Figs. 2(d)-2(f) show that the broadband correspond to the base angles of ~58° for both ZCG and HCG structures. The high reflectance areas in red for the middle and high Δn cases are roughly divided into two parts and the base angles near 60° yield the broadest bands. The reflectance is affected by refractive index difference, base angles, and thickness of the homogenous layer. High refractive index difference provides broader bands with base angles near $\alpha = \beta \approx 60°$ no matter what the homogenous-layer thickness is. In other words, this type of wideband guided-mode resonant reflectors will have quasi-equilateral triangle grating profiles for both ZCG and HCG structures.

4.2 Optimization of homogenous-layer thickness

Furthermore, we optimize the homogenous-layer thickness of the structure with quasi-equilateral triangle grating profiles. The reflectance maps $R_0(\lambda, d_h)$ are drawn versus wavelength and thickness for the period Λ = 850 nm. The base angles are changed to get optimized values for refractive index n = 3 and n = 3.48. Figures 3(a)-3(b) show the optimized values in black dotted lines. For n = 3, the optimized base angle is 59°, the optimized d_h is about 0.19 μm, and the broadband spans 230 nm from 1.28 μm to 1.51 μm. For n = 3.48, there are numerous broadband areas corresponding to different homogenous-layer thicknesses. Among them, the optimized d_h is about 0.54 μm and its broadband extends across 570 nm from 1.43 μm to 2.00 μm.

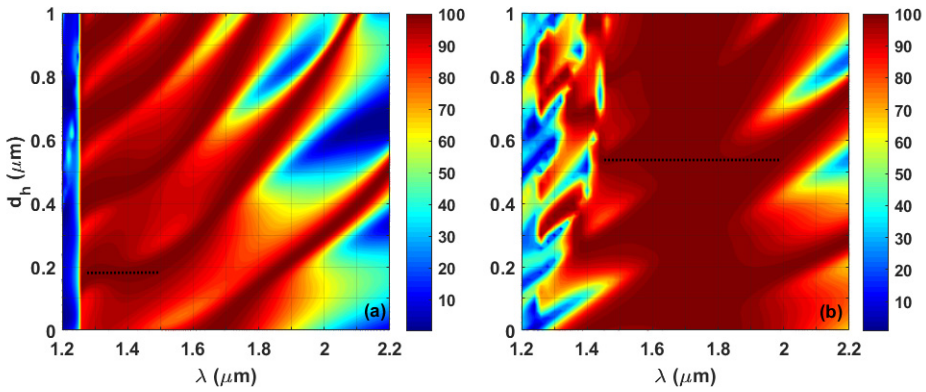

Fig. 3. The optimized reflectance map R_0 (λ, d_h) drawn versus wavelength and thickness for period Λ = 850 nm. (a) $\alpha = \beta$ = 59°, n_c = 1, n = 3, and n_s = 1.48; (b) $\alpha = \beta$ = 58°, n_c = 1, n = 3.48, and n_s = 1.48.

4.3 Characteristics of broadband ZCG and HCG reflectors

We design the ZCG broadband reflector with optimized parameters for TM polarization being Λ = 850 nm, d_h = 0.54 μm, $\alpha = \beta$ = 58° and n = 3.48. Figures 4(a) and 4(b) show the reflectance and transmittance spectrum comparison of ZCG and HCG on linear and

Optics EXPRESS

logarithmic scales. As seen in Fig. 4(a), for ZCG, the width of the reflection band with $R_0 >$ 99% is ~567 nm over the 1.432-1.999 μm range extending $\Delta\lambda/\lambda_{center}$ ≈33.3%. There exist three high-flat zones with $R_0 > 99.5\%$ around 1.45 μm, 1.70 μm and 1.95 μm inside the reflectance band and two reflectance dips with R_0 ≈99.0% at 1.52 μm and 1.84 μm between the high-flat zones. For the HCG, there are only two discontinuous bands with $R_0 > 99\%$ near 1.41 μm and 1.73 μm. Obviously, the reflectance and bandwidths of the ZCG are higher and broader than those for the HCG. Figure 4(b) quantifies the resonance locations, resonance amplitudes, and the spectral resonance separation.

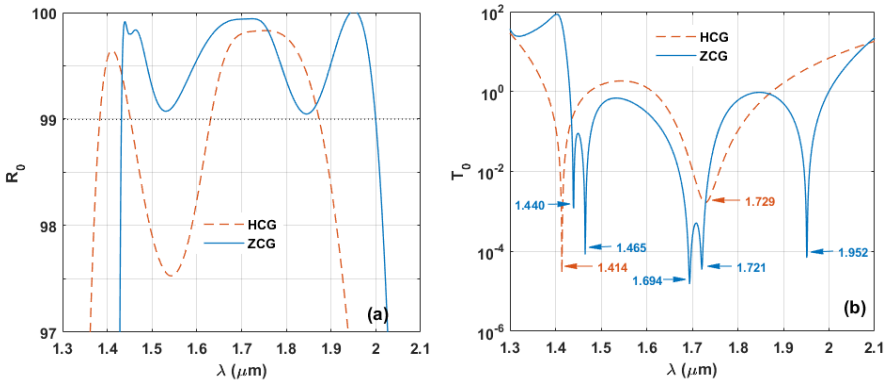

Fig. 4. Reflectance and transmittance spectra on (a) linear and (b) logarithmic scales comparing ZCGs and HCGs. The results are for TM polarization with Λ = 850nm, $\alpha = \beta = 58°$, $n_c = 1$, $n = 3.48$, and $n_s = 1.48$.

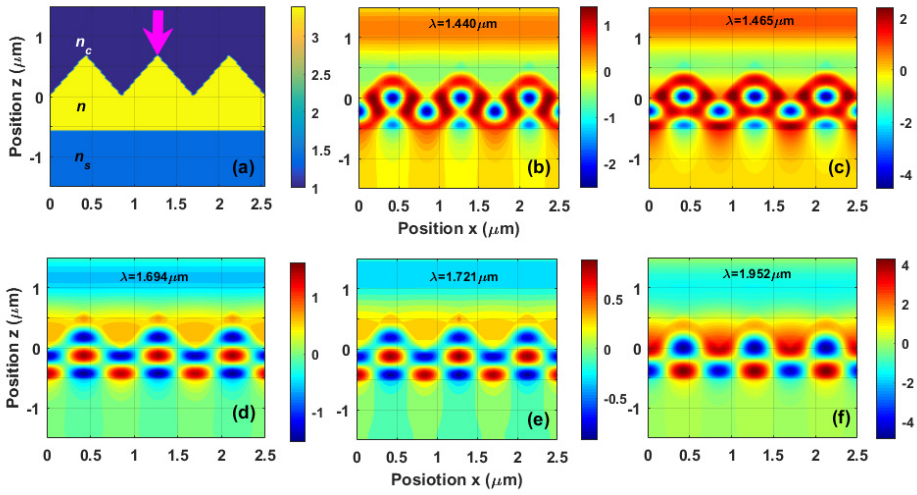

Fig. 5. Refractive index and internal magnetic field distributions in the ZCG structure and surrounding media at the resonance wavelengths for Λ = 850 nm, d_h = 540 nm, $\alpha = \beta = 58°$, and $n = 3.48$. (a) Refractive index; (b) λ = 1.440 μm; (c) λ = 1.465 μm; (d) λ = 1.694 μm; (e) λ = 1.721 μm; (f) λ = 1.952 μm. The scale bar measures the amplitude of the magnetic field.

In addition, Figs. 5(a)-5(f) display the refractive index distribution and internal magnetic field profiles associated with the five guided-mode resonance wavelengths in the ZCG structure and surrounding media. For the short wavelength λ = 1.440 and 1.465 μm in Figs. 5(b) and 5(c), the field distributions of the resonance pair are very similar, which locate in both the grating ridges and in the matched homogeneous layer. Simulating the fields at longer wavelengths λ = 1.694 and 1.721 μm in Figs. 5(d) and 5(e) shows that the fields are moved

Optics EXPRESS

forward almost entirely into the homogeneous layer and the high-low field distributions along the x and z axis are periodic. Finally, the field at λ = 1.952 μm locates mainly in the matched homogeneous layer in Fig. 5(f).

4.4 Tolerance of the optimized broadband reflector to the incident angle

Similar to rectangular gratings, Fig. 6(a) shows the angular sensitivity of the ZCG. It is rather sensitive to the incident angle and ± 1.2° deviation from normal splits the band into two bands both in the center and at its extremes. Figure 6(b) displays the sample at normal and deviated incidence (θ = + 5°). A narrow transmission gap emerges within the high reflectance spectra under off-normal incidence, yielding a resonance bandpass filter response. Figures 6(a) and 6(b) for this triangle GMR structure show a moderate tolerance range relative to incident angle.

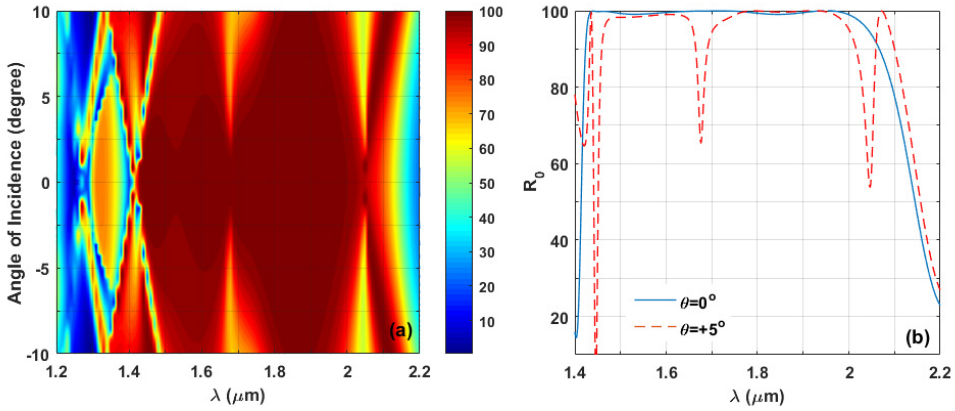

Fig. 6. (a) Angular sensitivity of the optimized broadband reflector. (b) Comparison of reflection spectra for normal (θ = 0°) and oblique (θ = + 5°) incidence.

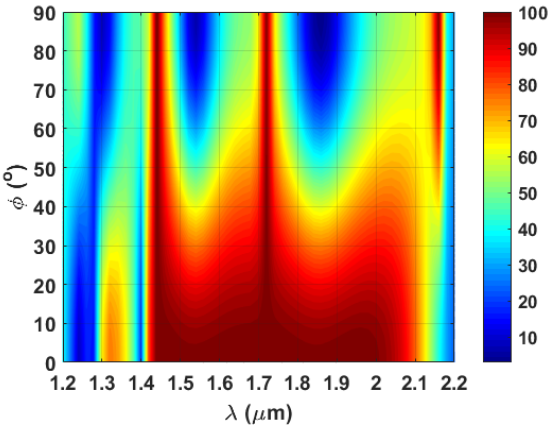

Fig. 7. Reflectance map $R_0(\lambda, \varphi)$ drawn versus wavelength and polarization angle for the optimized structure with Λ = 850 nm, $\alpha = \beta$ = 58°, n_c = 1, n = 3.48, and n_s = 1.48. φ = 0° corresponds to TM polarization and φ = 90° to TE polarization.

4.5 Effect of polarization state

For the optimized ZCG reflector, the tolerance of the broadband spectra to variation in input polarization angle ϕ is quantified in Fig. 7. Here, ϕ varies from 0° (TM polarization) to 90° (TE polarization). There exists a high reflectance broadband over the 1.44 - 1.99 μm range

Optics EXPRESS

within 4° of the polarization angle. The broadband narrows with increasing ϕ and it evolves into three single resonance wavelengths at 1.44 μm, 1.72 μm and 2.16 μm separately when the polarization state is TE. It shows that the optimized structure is suitable for TM polarization but with reasonable level of tolerance.

5. Conclusion

In this paper, focusing on the optical communication band, we have presented a model of a broadband guided-mode resonance (GMR) reflector with symmetric triangle grating profiles in TM polarization and studied the spectral properties, inner field distributions, and geometric characteristics of the devices in some detail by numerical simulations based on the coordinate transformation method (C method). The design parameters including refractive index n, base angle α, thickness of homogeneous layer d_h, and period are optimized to achieve high reflectance across wide flat bands. According to the simulations of the spectral characteristics of these reflectors with different n, α, and d_h, it is found that the optimized value of the base angles are close to 60°. When n = 3.48, the optimized base angle is $\alpha = \beta = 58°$. Based on these, we design broadband GMR reflectors by changing d_h and period Λ. Taking Λ = 850 nm for example, the width of the reflectance band with R_0>99% is ~567 nm over the 1.432-1.999 μm range with $\Delta\lambda/\lambda_{center}$ ≈33.3%. Clearly, similar to the GMR gratings with rectangular groove shapes, the ZCG type is superior in bandwidth to the HCG variety for triangular profiles. The inner magnetic field distributions for five resonance wavelengths for the optimal reflector are simulated. A plurality of resonance wavelengths with large resonance amplitudes result in broad reflection bands. In addition, we find that the quasi-equilateral triangle GMR structure provides tolerance range of incident angle within ± 1.2°. Moreover, there exists a high reflectance broadband over 550 nm within 4° of the design polarization angle which corresponds to TM polarization. Therefore, we can use the quasi-equilateral triangle GMR structure to design different broadband reflectors in different spectral bands by changing the period. These results will guide fabrication of broadband GMR reflectors with triangle grating profiles by grating ruling engines which may lead to economic ways to produce such devices for practical applications.

Funding

China Scholarship Council (CSC); Ministry of National Science and Technology through the National Key Basic Research Program of China (2014CB049500).